SUPPLEMENTARY METHODS

Model methodologies

We ran a suite of new ice-sheet model simulations to improve the chronological agreement between the timing of modelled retreat and that indicated by the new ^{14}C dates. The previously published model (Golledge et al., 2014) produced a mass-loss signature that closely replicated empirical records (Weber et al., 2014) for the early part of the glacial termination (18-11ka). However, the simulations predicted loss of grounded ice from the inner portions of the Ross and Weddell Sea embayments earlier than empirical data suggest (Anderson et al., 2014; Hillenbrand et al., 2014). We use emerging evidence of low mantle viscosity values (1e18 to 3e18 Pa S^{-1}) beneath parts of West Antarctica (Groh et al., 2012; Nield et al., 2012; van der Wal et al., 2015; Wiens et al., 2015) as the basis for our value of 5e18 Pa S^{-1}, but note that such low magnitudes are still poorly constrained. It is clear, however, that a value at least two orders of magnitude lower than that typical of East Antarctica is appropriate for our simulations, since nearly all of the ice volume loss occurs in areas underlain by West Antarctic, rather than East Antarctic, crust. The consequence on this sole modification is that crustal rebound takes place more quickly following grounded ice retreat. As a result, water depths are more rapidly reduced in marine areas and the retreating ice sheet stabilizes more easily. Because this feedback only occurs once ice is lost, the timing of initial retreat remains unaffected. However, as deglaciation progresses, the stabilizing effects of this isostatic feedback become more pronounced, effectively slowing ice-sheet retreat to an increasing degree through the Holocene. The new simulations are run at 10 km resolution and still produce a peak in mass loss at around the time of Meltwater Pulse (MWP) 1A, but yield a deglacial retreat in the Ross Sea that proceeds more slowly and reaches present-day grounding-lines at the Siple Coast in the late Holocene.

Cited References

Anderson, J.B., 1999, Antarctic Marine Geology: Cambridge University Press, UK.

Anderson, J.B., Conway, H., Bart, P.J., Witus, A.E., Greenwood, S.L., McKay, R.M., Hall, B.L., Ackert, R.P., Licht, K., Jakobsson, M., and Stone, J.O., 2014, Ross Sea paleo-ice sheet drainage and deglacial history during and since the LGM: Quaternary Science Reviews, v. 100, p. 31–54.

Baroni, C., and Hall, B.L., 2004, A new Holocene relative sea-level curve for Terra Nova Bay, Victoria Land, Antarctica: Journal of Quaternary Science, v. 19, no. 4, p. 377–396, doi: 10.1002/jqs.825.

Cowan, E.A., Seramur, K.C., Cai, J., and Powell, R.D., 1999, Cyclic sedimentation produced by fluctuations in meltwater discharge, tides and marine productivity in an Alaskan fjord: Sedimentology, v. 46, no. 6, p. 1109–1126, doi: 10.1046/j.1365-3091.1999.00267.x.

Domack, E.W., Jacobson, E.A., Shipp, S., and Anderson, J.B., 1999, Late Pleistocene-Holocene retreat of the West Antarctic Ice-Sheet system in the Ross Sea: Part 2--Sedimentologic and stratigraphic signature: Geological Society of America Bulletin, v. 111, no. 10, p. 1517–1536, doi: 10.1130/0016-7606(1999)111<1517:LPHROT>2.3.CO;2.

Ehrenberg, C., 1873, Microgeologische Studien uber das kleinste der Meeres-Tiefgrunde aller zonen und dessen geologischen einfluss: , p. 131–397.

Golledge, N.R., Menviel, L., Carter, L., Fogwill, C.J., England, M.H., Cortese, G., and Levy, R.H., 2014, Antarctic contribution to meltwater pulse 1A from reduced Southern Ocean overturning: Nature Communications, v. 5, doi: 10.1038/ncomms6107.

Groh, A., Ewert, M., Scheinert, M., Fritsche, A., Rulke, A., Richter, R., Rosenau, R., and Dietrich, R., 2012, An investigation of Glacial Isostatic Adjustment over the Amundsen Sea sector, West Antarctica.: Global and Planetary Change, v. 98-99, p. 45–53, doi: doi:10.1016/j.gloplacha.2012.08.001.

Hall, B.L., Baroni, C., and Denton, G.H., 2004, Holocene relative sea-level history of the Southern Victoria Land Coast, Antarctica: Global and Planetary Change, v. 42, no. 1–4, p. 241–263, doi: 10.1016/j.gloplacha.2003.09.004.

Hall, B.L., Henderson, G.M., Baroni, C., and Kellogg, T.B., 2010, Constant Holocene Southern-Ocean 14C reservoir ages and ice-shelf flow rates: Earth and Planetary Science Letters, v. 296, no. 1–2, p. 115–123, doi: 10.1016/j.epsl.2010.04.054.

Hemer, M.A., and Harris, P.T., 2003, Sediment core from beneath the Amery Ice Shelf, East Antarctica, suggests mid-Holocene ice-shelf retreat: Geology, v. 31, no. 2, p. 127–130, doi: 10.1130/0091-7613(2003)031<0127:SCFBTA>2.0.CO;2.

Hillenbrand, C.-D., Bentley, M.J., Stolldorf, T.D., Hein, A.S., Kuhn, G., Graham, A.G.C., Fogwill, C.J., Kristoffersen, Y., Smith, J.A., Anderson, J.B., Larter, R.D., Melles, M., Hodgson, D.A., Mulvaney, R., et al., 2014, Reconstruction of changes in the Weddell Sea sector of the Antarctic Ice Sheet since the Last Glacial Maximum: Quaternary Science Reviews, v. 100, p. 111–136, doi: 10.1016/j.quascirev.2013.07.020.

Kanmachefr, F., 1798, Adam's Essays on the Microscope: The Second Edition, with Considerable Additions and Improvements.: Dillon and Keating, London.

Licht, K.J., Jennings, A.E., Andrews, J.T., and Williams, K.M., 1996, Chronology of late Wisconsin ice retreat from the western Ross Sea, Antarctica: Geology, v. 24, no. 3, p. 223–226, doi: 10.1130/0091-7613(1996)024<0223:COLWIR>2.3.CO;2.

McKay, R., Browne, G., Carter, L., Cowan, E., Dunbar, G., Krissek, L., Naish, T., Powell, R., Reed, J., Talarico, F., and Wilch, T., 2009, The stratigraphic signature of the late Cenozoic Antarctic Ice Sheets in the Ross Embayment: Geological Society of America Bulletin, v. 121, no. 11-12, p. 1537–1561, doi: 10.1130/B26540.1.

McKay, R.M., Dunbar, G.B., Naish, T.R., Barrett, P.J., Carter, L., and Harper, M., 2008, Retreat history of the Ross Ice Sheet (Shelf) since the Last Glacial Maximum from deep-basin sediment cores around Ross Island: Palaeogeography, Palaeoclimatology, Palaeoecology, v. 260, no. 1-2, p. 245–261, doi: 10.1016/j.palaeo.2007.08.015.

Nield, G.A., Barletta, V.R., Bordoni, A., King, M.A., Whitehouse, P.L., Clarke, P.J., Domack, E., Scambos, T.A., and Berthier, E., 2012, Rapid bedrock uplift in the Antarctic Peninsula explained by viscoelastic response to recent ice unloading.: Earth and Planetary Science Letters, v. 397, p. 32–41, doi: doi:10.1016/j.epsl.2014.04.019.

d'Orbigny, A.D., 1826, Tableau méthodique de la classe des Céphalopodes.: v. 7, p. 245–314.

Parr, W.J., 1950, Foraminifera: v. 5, p. 235–392.

Smith, J.A., Hillenbrand, C.-D., Kuhn, G., Larter, R.D., Graham, A.G.C., Ehrmann, W., Moreton, S.G., and Forwick, M., 2011, Deglacial history of the West Antarctic Ice Sheet in the western Amundsen Sea Embayment: Quaternary Science Reviews, v. 30, no. 5-6, p. 488–505, doi: 16/j.quascirev.2010.11.020.

Stuvier, M., and Reimer, J., 1993, Extended 14C data base and revised CALIB 3.014 C age calibration program: Radiocarbon, v. 35, p. 215–230.

van der Wal, W., Whitehouse, P., and Schrama, E., 2015, Effect of GIA models with 3D composite mantle viscosity on GRACE mass balance estimates for Antarctica.: Earth and Planetary Science Letters, v. 414, p. 134–143.

Weber, M.E., Clark, P.U., Kuhn, G., Timmermann, A., Sprenk, D., Gladstone, R., Zhang, X., Lohmann, G., Menviel, L., Chikamoto, M.O., Friedrich, T., and

Ohlwein, C., 2014, Millennial-scale variability in Antarctic ice-sheet discharge during the last deglaciation: Nature, v. 510, no. 7503, p. 134–138, doi: 10.1038/nature13397.

Wiens, D., Heeszel, D., Aster, R., Nyblade, A., and Wilson, T., 2015, Seismic Constraints on the Mantle Viscosity Structure beneath Antarctica. Vol. 17, EGU2015-7738, 2015, *in* Geophysical Research Abstracts, Geophysical Research Abstracts.

Supplementary Figure Legend

Figure DR1. X-radiographs of the facies succession documented in core CH-GC-08. A) Diatom ooze (Facies DO) at 7-12 centimetres below seafloor (cmbsf), showing abundant clasts and bioturbation. B) Laminated Mud (Facies Ml) at 38-42 cmbsf showing rhythmic sub mm-scale laminae. C) Laminated Mud with Clasts (Facies Mc) at 55-60 cmbsf showing gravel sized clasts within muds containing rhythmic sub-mm-scale laminae. D) Laminated Mud (Facies Ml) at 68-73 cmbsf showing rhythmic sub mm-scale laminae. E) Stratified Diamict (Facies Ds) at 87-92 cmbsf. F) Massive Diamict (Facies Dm) at 92-97 cmbsf.

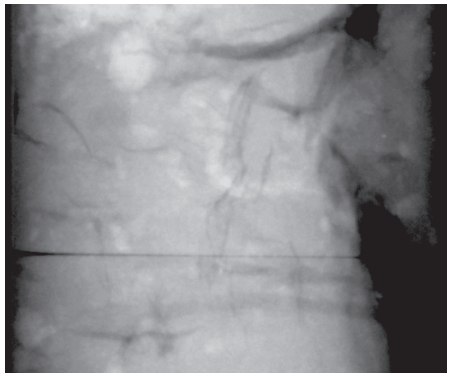

A - Facies DO (7-12cmbsf)

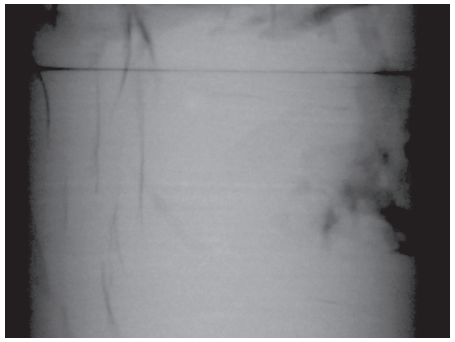

B- Facies Ml (38-42cmbsf)

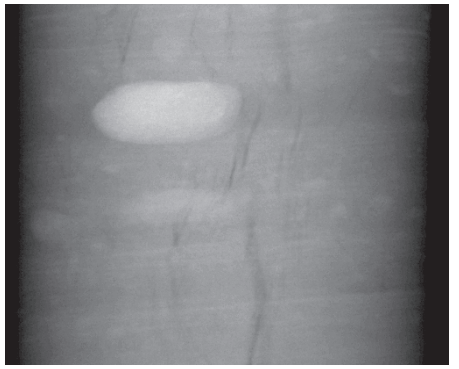

C - Facies Mc(55-60 cmbsf)

D - Facies Ml (68-73 cmbsf)

E - Facies Ds (78-83 cmbsf)

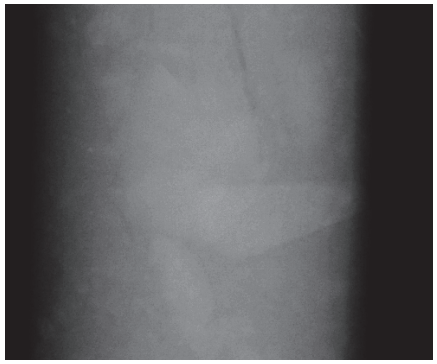

F- Facies Dm (92-97 cmbsf)

Figure DR1

TABLE DR1. FACIES DESCRIPTIONS AND INTERPRETATIONS. SEE FIGURE 2 IN MAIN TEXT FOR ADDITIONAL DETAIL ON PROXIES.

Facies	Lithology and Sedimentary features	Clast lithologies	Fossil content	Interpretation
DO	Bioturbated diatom ooze with abundant clasts (DO). High opal (20-25%), TOC content (>0.5%), and high water content (~40-50%),	Granite, rounded quartz, quartz, feldspars, dolerite, foliated/mylontic granitoids, basalt	high diatom abundance (1.4 x10^9 valves/g), benthic foraminifera.	Pelagic sedimentation with ice rafted debris. General lack of terrigenous material. Thin bioturbated interval with abundant clasts suggests winnowing and current reworking (Domack et al., 1999) and is likely a condensed section. At the time of coring the site was 15 km south of the calving line, but was ~5km from the calving line when C-19 (a 200x32 km iceberg) calved off in 2002. This effectively places the CH-2 in the modern day "calving zone" of the Ross Ice Shelf since the ice shelf became pinned to Ross Island during the glacial retreat. The presence of gravel clasts indicates open water with ice rafting must have existed at numerous time through the Holocene, as the base of the Ross Ice Shelf at this site was observed by video observations during hot water drilling to be free of basal debris.
Mb	Bioturbated mud. Moderate opal (~10), TOC content (~0.25%), and high water content (~50%).	Absent	moderate diatom abundance (0.5x10^9 valves/g)	Hemipelagic suspension settling. Bioturbation is the likely result of decrease sediment supply as the grounding line migrated away from the core site, allowing for the establishment of a benthos community (Domack et al., 1999; Hemer and Harris, 2003). The lack of outsized clasts is indicative of depostion beneath an ice shelf lacking basal debris (Domack et al., 1999, Hemer and Harris, 2003; Mckay et al., 2009)
Mc	Mud with highly rhythmic, but faint sub-mm- to mm-scale laminae and common gravel-sized clasts. Moderate opal (~10), TOC content (~0.25%), and high water content (~45%),	quartz, feldspars, granite,basalt, dolerite,metamorphic lithologies (foliated/mylontic granitoids, metasediments, marble)	Benthic/planktic foraminifera*, Common diatoms (0.74x10^9 valves/g)	Common diatom content and gravel clasts alongside the planktonic/benthic foraminifera suggests a short duration period of pelagic sedimentation in open water with iceberg rafting over the core site. Rhythmic laminae suggest traction currents reworking hemipelagic suspension settling sediments or turbidites (see facies Ml). We interpret that the input of terrigenous material has allowed this short-lived interval to be preserved in the stratigraphy, where as higher in the stratigraphic succession (e.g. Facies Mb), sediment starvation (due to a lack of terrigenous sediment supply) combined with bioturbation does not allow for the preservation of such events.
Ml	Mud with highly rhythmic, but faint sub-mm- to mm-scale laminae defined by colour rather than obvious grainsize variations. Moderate opal (~10%), TOC content (~0.25%), and high water content (~40-50%).	Absent	moderate diatom abundance (0.5x10^9 valves/g)	Rhythmic laminae suggest influence of traction currents reworking hemipelagic suspension settling sediments or turbidites . Rhythmites can also interpreted as meltwater plumes, but thin nature of facies, and lack of obvious size sorting argues against this interpretation, as plumites are often associated with large volume of subglacial meltwater release and high sedimentation rates (Cowan et al., 1999; McKay et al., 2009). Increased opal and TOC consistent with sub ice shelf setting (Hemer and Harris, 2003). The lack of outsized clasts is indicative of depostion beneath an ice shelf lacking basal debris (Domack et al., 1999, Hemer and Harris, 2003; Mckay et al., 2009)
Ds	weakly-stratified muddy diamict with common granule-sized intraclasts of mud and diamict. TOC (0.27-0.37%), low water content (25-30%)	quartz, dolerite, granite,metamorphic lithologies (foliated/mylontic granitoids, metasediment, biotite schists, marble)	Highly fragmented diatom (0.4x10^9 valves/g)	Glacimarine sediment deposited proximal to grounding line by melt out of subglacial basal debris. A lower sand content than Facies Dm suggest some water sorting during deposition, while the slightly elevated diatom abundance, water content and TOC compared to the underlying massive diamict suggest an increasing marine influence. (Domack et al., 1999). Common intraclasts are consistent with the granulated facies of

Domack et al., 1999.

Dm	Muddy Diamict, low opal (5%), TOC content (<0.25%), and low water content (~15-20%).	quartz, dolerite, granite,metamorphic lithologies (foliated/mylontic granitoids, metasediments, biotite schists, marble)	Highly fragmented diatom ($0.3x10^9$ valves/g)	Subglacial transport and deposition in a subglacial or a grounding line proximal depositional setting (i.e. subglacial basal debris melt out). Lowest values of diatom and opal (but still high relative to other tills in antarctica, suggesting reworking of older diatom oozes), TOC and water content similar to other diamicts interpreted as tills elsewhere in the Ross Sea (Licht et al., 1996; Anderson, 1999; Domack et al., 1999, Mckay et al., 2008) and the Antarctic margin ((Smith et al., 2011)).

*All foram species have previously been reported in the Ross Sea by Ward and Webb, 1986. *Neogloboquadrina pachyderma* (Ehrenberg, 1873). *Lagena* spp. (Walker and Jacob (in Kanmachefr, (1798)), *Astrononion antarcticus* (Parr, 1950), *Cibicides lobatulus* (Walker and Jacob (in Kanmachefr, (1798)), *Rosalina globularis* ((d'Orbigny, 1826))

Table DR2. Reported and calibrated radiocarbon dates used in this study*

Core	Sample depth (cm)	Laboratory code	dated material	Convential ^{14}C age (yrs BP)± error (1 sigma)	ΔR (yrs)	ΔR ± error	Calibrated age ± error
CHGC-08	1.5-2.5	NZA37586	AIO	13573 ± 50	N/A	N/A	N/A
CHGC-08	10-11	NZA37626	AIO	10074 ± 35 BP	N/A	N/A	N/A
CHGC-08	17-18	NZA37625	AIO	16018 ± 55 BP	N/A	N/A	N/A
CHGC-08	23-24	NZA 37585	AIO	25100 ± 150	N/A	N/A	N/A
CHGC-08	27-28	NZA37624	AIO	31390 ± 310	N/A	N/A	N/A
CHGC-08	32-33	NZA 37584	AIO	28870 ± 230	N/A	N/A	N/A
CHGC-08	46-47	NZA37623	AIO	32190 ± 350	N/A	N/A	N/A
CHGC-08	59-60	NZA 37583	AIO	29130 ± 240	N/A	N/A	N/A
CHGC-08	71-72	NZA37590	AIO	33210 ± 390	N/A	N/A	N/A
CHGC-08	75-76	NZA37589	AIO	26240 ± 170	N/A	N/A	N/A
CHGC-08	79-80	NZA 37582	AIO	35250 ± 510	N/A	N/A	N/A
CHGC-08	88-89	NZA37938	AIO	26210±180	N/A	N/A	N/A
CHGC-08	101-102	NZA37581	AIO	33050±390	N/A	N/A	N/A
CHGC-07	50-54	NZA 50805	*N.Pachyderma* (planktic foram.)	8726 ± 105	791	121	8391±179.5
CHGC-07	50-54	NZA50804	benthic foram.	8892 ± 155	791	121	8616±242
Previous studies (mentioned in text)							
DF80-189 (McKay et al., 2008)	127–129	NZA25913	AIO (bulk)	11331±45	2070†	N/A	10100±74
DF80-57 (Licht et al., 1996)	43	AA11876	Reworked shell	7830 ± 60	791	121	7530±117
Terra Nova Bay (Baroni and Hall, 2004)	Adelie Cove	TO-5571 (4)	Penguin guano	8490 ± 90	791	121	8161±151
Scott Coast (Hall et al., 2004)	N/A	N/A	Modelled beach uplift§	7750+150	791	121	7455±125

Note. *Bulk sediment ages are not corrected for reservoir effect or calibrated, due to inherent uncertainties with reworking of carbon in these dates (see main text). Carbonate ages are corrected and calibrated and based on foraminifera collected from the sieved >63 micron fraction. Planktonic species are dominated by *Neogloboquadrina pachyderma* (100 specimens used for dating), but there is a more diverse assemblage of benthic species (340 specimens used for dating), as listed in Table DR1. Calibration of all marine ^{14}C dates was conducted in Calib 7.1 (Stuvier and Reimer, 1993) using a 1144 year reservoir age correction (Hall et al., 2010) and the Marine13 calibration (n.b. ΔR of 791±121 is the value used in the CALIB 7.1 program as defined by Hall et al., (2010)).

† This AIO date is corrected by subtraction of core top sediment (2470 ^{14}C years BP). ΔR **value accounts for built in 400 yr correction in Calib 7.1. Age is not used in our interpretation, but to highlight issue with AIO ages.**

§ Age is based on modeled relative sea level curve (6450±150 ^{14}C years BP, corrected with a 1300 year reservoir age) derived from raised beach. This revised estimate uses the 1144 reservoir correction.

Table DR3. Grain size, water content, diatom abundance, Total Organic Carbon (TOC) and biogenic opal for CH-GC-08

depth (cmbsf)	%mud	%sand	%gravel	water content(%)	diatoms (v/gx109)	TOC %	biogenic opal %
0.00	69.55	29.76	0.69	46.12			
2.00						0.62	21.00
3.00	68.55	27.81	3.64	45.11			
4.00					1.82		
6.00	58.25	23.77	17.97	37.45			
7.00						0.55	19.30
8.00	80.65	16.43	2.92	50.13			
9.00					1.46		
12.00	83.93	15.13	0.94	51.29			
12.00						0.47	21.40
14.00					1.37		
15.00	91.13	8.14	0.74	49.71			
18.00	97.07	2.68	0.25	48.70			
19.00						0.55	24.10
21.00	96.80	3.20	0.00	47.80			
21.00					1.07		
24.00	96.88	3.12	0.00	42.22			
25.00						0.27	12.60
27.00					0.58		
28.00	98.90	1.10	0.00	45.67			
29.00						0.27	12.70
31.00	99.97	0.03	0.00	51.03			
32.00					0.46		
33.00	99.95	0.05	0.00	49.32			
34.00						0.26	9.20
36.00	99.80	0.20	0.00	51.39			
37.00						0.27	10.10
39.00	99.93	0.07	0.00	49.44			
39.00					0.43		
42.00	98.18	1.82	0.00	45.73			
43.00						0.25	8.80
45.00	99.42	0.58	0.00	46.69			
45.00					0.37		
48.00	97.51	2.49	0.00	46.38			
49.00					0.51		
49.00						0.25	8.80
51.00	90.47	9.53	0.00	40.38			
52.00					0.59		
53.00	88.39	11.44	0.18	41.40			
54.00					0.61		
55.00						0.26	7.70
57.00	80.13	11.38	8.49	37.80			
57.00					0.75		
59.00					0.74		
60.00	93.92	6.08	0.00	42.25			
60.00					0.54		
61.00						0.31	9.80
62.00	90.56	9.44	0.00	42.71			
63.00					0.49		
64.00	94.51	5.49	0.00	43.37			
65.00						0.30	8.60
67.00	97.75	2.25	0.00	43.19			
67.00					0.46		
70.00	99.63	0.37	0.00	43.00			
70.00						0.34	7.90
73.00	99.83	0.17	0.00	51.82			
74.00					0.47		
74.00						0.39	10.80
76.00	99.45	0.55	0.00	48.84			
78.00						0.37	7.80
80.00	68.51	22.36	9.13	30.00			
80.00					0.39		
83.00	76.76	22.34	0.90	28.50			
84.00						0.28	5.80
86.00	73.84	24.29	1.87	24.12			
86.00					0.37		
89.00						0.22	4.20
90.00	62.41	33.75	3.84	19.04			
92.00					0.33		
93.00	73.76	22.28	3.96	14.79			
93.00						0.23	4.20
96.00	62.89	33.63	3.48	17.03			
98.00						0.24	5.80
99.00	59.53	35.08	5.39	19.09			
99.00					0.29		
102.00	60.52	35.16	4.32	19.39			
103.00						0.22	4.80
104.00	65.39	32.75	1.87	20.44			
105.00					0.27		
107.00	65.01	34.23	0.76	21.43			

Table DR4. Physical Property measurements for CH-GC-08

Depth (cmbsf)	Density (gm/cc)	Magnetic Suspectibility (SI)
0	1.2933	30.1197
0.5	1.23	
1	1.1884	36.6227
1.5	1.2107	
2	1.2553	40.5387
2.5	1.2621	
3	1.2626	43.0049
3.5	1.2981	
4	1.3414	43.8736
4.5	1.3625	
5	1.3627	43.6777
5.5	1.3861	
6	1.4352	42.9793
6.5	1.516	
7	1.4357	41.6262
7.5	1.3788	
8	1.3398	39.859
8.5	1.3828	
9	1.3803	38.3832
9.5	1.3735	
10	1.3749	37.4175
10.5	1.4079	
11	1.4111	36.9181
11.5	1.3971	
12	1.3972	36.9731
12.5	1.4564	
13	1.468	37.3871
13.5	1.466	
14	1.4648	38.1784
14.5	1.4516	
15	1.451	39.1674
15.5	1.4556	
16	1.4398	40.2563
16.5	1.4331	
17	1.4309	41.0699
17.5	1.4441	
18	1.4467	42.1875
18.5	1.4485	
19	1.4691	42.7845
19.5	1.4633	
20	1.4747	43.6889
20.5	1.4731	
21	1.47	44.066
21.5	1.4961	
22	1.5183	44.0879
22.5	1.52	
23	1.5379	43.9758
23.5	1.5406	
24	1.5573	43.2899
24.5	1.5402	
25	1.5253	41.7978
25.5	1.5073	
26	1.4916	40.098
26.5	1.4914	
27	1.4851	38.179
27.5	1.4808	
28	1.4597	36.1082
28.5	1.4609	
29	1.4698	34.7117
29.5	1.4502	
30	1.469	33.6975
30.5	1.459	
31	1.4423	33.731
31.5	1.4476	
32	1.4414	33.9475
32.5	1.4479	
33	1.4274	34.1642
33.5	1.4422	
34	1.4682	34.5809
34.5	1.4886	
35	1.488	34.5637
35.5	1.4892	
36	1.4831	34.9807
36.5	1.472	
37	1.4428	34.9807
37.5	1.424	
38	1.374	35.1806
38.5	1.2153	
39	1.2281	35.9365
39.5	1.4026	
40	1.465	36.6151
40.5	1.4713	
41	1.4675	37.4056
41.5	1.4732	

42	1.483	37.8987
42.5	1.5207	
43	1.532	37.7668
43.5	1.5368	
44	1.5435	37.6729
44.5	1.5214	
45	1.5178	37.7229
45.5	1.5043	
46	1.4988	37.6854
46.5	1.4943	
47	1.5147	37.7907
47.5	1.463	
48	1.4239	38.1885
48.5	1.4214	
49	1.4626	39.183
49.5	1.5372	
50	1.551	39.6811
50.5	1.5608	
51	1.5712	40.8715
51.5	1.5668	
52	1.5631	41.8428
52.5	1.5557	
53	1.5571	42.3325
53.5	1.5628	
54	1.5584	42.5303
54.5	1.5791	
55	1.6249	42.7281
55.5	1.6263	
56	1.6081	42.8196
56.5	1.5848	
57	1.598	42.8196
57.5	1.5882	
58	1.5809	42.4957
58.5	1.5843	
59	1.5702	41.8225
59.5	1.5261	
60	1.5205	41.0371
60.5	1.5361	
61	1.5487	40.2318
61.5	1.5457	
62	1.5301	39.8393
62.5	1.5243	
63	1.5207	39.27
63.5	1.5123	
64	1.5341	38.5036
64.5	1.542	
65	1.5364	37.6992
65.5	1.5201	
66	1.5243	36.6266
66.5	1.503	
67	1.4937	35.5217
67.5	1.5063	
68	1.5034	34.8747
68.5	1.5054	
69	1.5165	33.2654
69.5	1.504	
70	1.501	31.8876
70.5	1.5015	
71	1.4851	30.9034
71.5	1.457	
72	1.4459	29.9192
72.5	1.4517	
73	1.4619	29.1463
73.5	1.4586	
74	1.4616	29.4015
74.5	1.456	
75	1.4739	30.9801
75.5	1.4547	
76	1.4778	34.0242
76.5	1.4737	
77	1.5273	38.3762
77.5	1.5951	
78	1.6756	44.0023
78.5	1.7568	
79	1.7438	49.9733
79.5	1.7217	
80	1.7422	55.9225
80.5	1.7514	
81	1.7485	61.582
81.5	1.7714	
82	1.761	66.3992
82.5	1.7836	
83	1.7844	70.0471
83.5	1.7814	
84	1.7621	74.0271
84.5	1.7512	

85	1.7286	77.8467
85.5	1.753	
86	1.8186	81.91
86.5	1.8649	
87	1.8394	85.7527
87.5	1.8691	
88	1.8884	88.327
88.5	1.8916	
89	1.8878	89.9974
89.5	1.8661	
90	1.8843	92.4831
90.5	1.9001	
91	1.8826	96.4074
91.5	1.8808	
92	1.8948	101.5002
92.5	1.9042	
93	1.8917	105.5886
93.5	1.8818	
94	1.8599	104.5792
94.5	1.8909	
95	1.8854	100.4376
95.5	1.8725	
96	1.8671	95.7802
96.5	1.8547	
97	1.8486	91.3652
97.5	1.8445	
98	1.8411	88.0065
98.5	1.8341	
99	1.8277	84.9752
99.5	1.8279	
100	1.8239	81.7988
100.5	1.8295	
101	1.8839	78.1062
101.5	1.9697	
102	1.9984	69.8731
102.5	1.9902	
103	1.9712	61.3288
103.5	1.9483	
104	1.8809	48.0274
104.5	1.8406	
105	1.7669	37.9542
105.5	1.6494	
106	1.3446	27.8093
106.5	1.1324	
107	1.0171	18.7546

Table DR5. Physical Property measurements for CH-GC-07

Depth (cmbsf)	Density (gm/cc)	Magnetic Susceptibility (SI)
0	0.8274	23.6084
0.5	1.4733	
1	1.5292	33.0786
1.5	1.4781	
2	1.4615	41.0647
2.5	1.4712	
3	1.4477	46.0545
3.5	1.4429	
4	1.4469	49.2833
4.5	1.4392	
5	1.3302	51.216
5.5	1.2443	
6	1.3144	52.531
6.5	1.4308	
7	1.4426	52.5051
7.5	1.4747	
8	1.4744	51.6893
8.5	1.4786	
9	1.452	49.5762
9.5	1.4219	
10	1.4246	47.8445
10.5	1.4264	
11	1.4511	46.5696
11.5	1.4443	
12	1.4004	44.635
12.5	1.414	
13	1.4465	44.1787
13.5	1.466	
14	1.4305	44.2883
14.5	1.4001	
15	1.4229	44.0036
15.5	1.4246	
16	1.439	43.4547
16.5	1.5151	
17	1.4947	42.9472
17.5	1.4841	
18	1.4907	42.4587
18.5	1.5058	
19	1.5113	41.9369
19.5	1.5104	
20	1.495	41.5618
20.5	1.4998	
21	1.5077	41.4795
21.5	1.5235	
22	1.5308	41.6977
22.5	1.5114	
23	1.5102	41.6563
23.5	1.5051	
24	1.5203	41.833
24.5	1.511	
25	1.5065	42.1649
25.5	1.5071	
26	1.5108	42.144
26.5	1.5201	
27	1.5201	42.144
27.5	1.5441	
28	1.5511	42.0605
28.5	1.556	
29	1.5429	41.8225
29.5	1.5405	
30	1.5577	41.4298
30.5	1.5502	
31	1.5536	40.9356
31.5	1.5365	
32	1.5299	40.2318
32.5	1.5116	
33	1.5032	39.4859
33.5	1.5032	
34	1.498	38.1935
34.5	1.4695	
35	1.4697	37.7084
35.5	1.4728	
36	1.4765	37.8205
36.5	1.4848	
37	1.4908	38.1369
37.5	1.5024	
38	1.5219	39.1705
38.5	1.5264	
39	1.5232	40.4919
39.5	1.5134	
40	1.5217	41.2819
40.5	1.5065	
41	1.5162	41.833
41.5	1.5295	

42	1.5299	42.1231
42.5	1.479	
43	1.4302	41.8823
43.5	1.5032	
44	1.5232	41.986
44.5	1.5138	
45	1.5009	41.4927
45.5	1.5146	
46	1.4867	40.8073
46.5	1.4575	
47	1.4356	39.951
47.5	1.4467	
48	1.4915	39.4276
48.5	1.4431	
49	1.3197	38.8641
49.5	1.2782	
50	1.4435	39.4471
50.5	1.5528	
51	1.5292	40.0498
51.5	1.5244	
52	1.5613	40.9611
52.5	1.545	
53	1.5549	41.7871
53.5	1.5702	
54	1.5659	42.7544
54.5	1.5532	
55	1.5373	44.3239
55.5	1.5255	
56	1.5378	46.0887
56.5	1.5267	
57	1.5366	48.2188
57.5	1.5682	
58	1.5994	51.0127
58.5	1.6063	
59	1.6042	52.5184
59.5	1.6245	
60	1.6054	52.5184
60.5	1.63	
61	1.6022	51.3514
61.5	1.5527	
62	1.5547	49.553
62.5	1.5618	
63	1.5535	47.6728
63.5	1.5437	
64	1.5417	45.9598
64.5	1.5612	
65	1.5657	44.5908
65.5	1.5268	
66	1.5273	43.0262
66.5	1.521	
67	1.5311	41.3683
67.5	1.5247	
68	1.5279	39.702
68.5	1.5125	
69	1.5137	38.0461
69.5	1.5099	
70	1.5125	36.4509
70.5	1.5184	
71	1.499	34.9613
71.5	1.4888	
72	1.4857	33.86
72.5	1.4685	
73	1.4614	32.9516
73.5	1.4723	
74	1.4886	32.9844
74.5	1.4863	
75	1.4774	34.7554
75.5	1.4838	
76	1.462	38.3684
76.5	1.4801	
77	1.4778	44.2434
77.5	1.5195	
78	1.5776	52.2232
78.5	1.5856	
79	1.5944	61.0878
79.5	1.6177	
80	1.6726	69.174
80.5	1.808	
81	1.9504	75.3942
81.5	1.9668	
82	1.9748	79.6275
82.5	1.9373	
83	1.9365	82.0466
83.5	1.8947	
84	1.9074	81.8064
84.5	1.9115	

85	1.9296	80.2704
85.5	1.9504	
86	1.9295	76.8715
86.5	1.95	
87	1.9891	71.2318
87.5	1.9761	
88	1.9359	61.7645
88.5	1.9147	
89	1.5765	47.8212
89.5	1.2477	